J Arid Land (2025) 17(1): 1–18
doi: 10.1007/s40333-025-0071-1; CSTR: 32276.14.JAL.02500711

Science Press Springer-Verlag

Runoff simulation and hydropower resource prediction of the Kaidu River Basin in the Tianshan Mountains, China

ZHANG Jing, XU Changchun*, WANG Hongyu, WANG Yazhen, LONG Junchen

College of Geography and Remote Sensing Science, Xinjiang University, Urumqi 830017, China

Abstract: The Tianshan Mountains of Central Asia, highly sensitive to climate change, has been comprehensively assessed for its ecosystem vulnerability across multiple aspects. However, studies on the region's main river systems and hydropower resources remain limited. Thus, examining the impact of climate change on the runoff and gross hydropower potential (GHP) of this region is essential for promoting sustainable development and effective management of water and hydropower resources. This study focused on the Kaidu River Basin that is situated above the Dashankou Hydropower Station on the southern slope of the Tianshan Mountains, China. By utilizing an ensemble of bias-corrected global climate models (GCMs) from Coupled Model Intercomparison Project Phase 6 (CMIP6) and the Variable Infiltration Capacity (VIC) model coupled with a glacier module (VIC–Glacier), we examined the variations in future runoff and GHP during 2017–2070 under four shared socio-economic pathway (SSP) scenarios (SSP1-2.6, SSP2-4.5, SSP3-7.0, and SSP5-8.5) compared to the baseline period (1985–2016). The findings indicated that precipitation and temperature in the Kaidu River Basin exhibit a general upward trend under the four SSP scenarios, with the fastest rate of increase in precipitation under the SSP2-4.5 scenario and the most significant changes in mean, maximum, and minimum temperatures under the SSP5-8.5 scenario, compared to the baseline period (1980–2016). Future runoff in the basin is projected to decrease, with rates of decline under the SSP1-2.6, SSP2-4.5, SSP3-7.0, and SSP5-8.5 scenarios being 3.09, 3.42, 7.04, and 7.20 m^3/s per decade, respectively. The trends in GHP are consistent with runoff, with rates of decline in GHP under the SSP1-2.6, SSP2-4.5, SSP3-7.0, and SSP5-8.5 scenarios at 507.74, 563.33, 1158.44, and 1184.52 MW/10a, respectively. Compared to the baseline period (1985–2016), the rates of change in GHP under the SSP1-2.6, SSP2-4.5, SSP3-7.0, and SSP5-8.5 scenarios are –20.66%, –20.93%, –18.91%, and –17.49%, respectively. The Kaidu River Basin will face significant challenges in water and hydropower resources in the future, underscoring the need to adjust water resource management and hydropower planning within the basin.

Keywords: climate change; runoff; gross hydropower potential (GHP); Coupled Model Intercomparison Project Phase 6 (CMIP6); Variable Infiltration Capacity (VIC) model coupled with a glacier module (VIC–Glacier); Kaidu River Basin

Citation: ZHANG Jing, XU Changchun, WANG Hongyu, WANG Yazhen, LONG Junchen. 2025. Runoff simulation and hydropower resource prediction of the Kaidu River Basin in the Tianshan Mountains, China. Journal of Arid Land, 17(1): 1–18. https://doi.org/10.1007/s40333-025-0071-1; https://cstr.cn/32276.14.JAL.02500711

1 Introduction

Energy forms the material foundation and driving force behind socio-economic development and serves as a critical battleground for achieving the goals of "carbon peak and carbon neutrality"

*Corresponding author: XU Changchun (E-mail: xucc@xju.edu.cn.cn)
Received 2024-05-13; revised 2024-11-17; accepted 2024-11-25

(Yuan et al., 2022). Clean energy sources, including wind, solar, and hydropower, have attracted significant attention due to their indispensable role in mitigating climate change and reducing greenhouse gas emissions (Jing et al., 2024; Li et al., 2024). Among these, hydropower is a cornerstone of clean energy systems, playing an essential role in global decarbonization efforts (Mohsin et al., 2023). China, endowed with some of the world's richest hydropower resources, exhibits tremendous potential, with a theoretical total hydropower capacity of 694 GW, a technically exploitable capacity of 542 GW, and an economically feasible potential of 402 GW (Sun et al., 2019). The development of hydropower resources has been instrumental in addressing the energy crisis and mitigating environmental pollution, both of which have intensified alongside China's rapid economic growth in the 21st century (Melo et al., 2019). However, in the face of global climate change, hydropower resources are encountering unprecedented challenges (Donk et al., 2018; Zhong et al., 2019; Jian et al., 2023). The impacts of climate change on hydropower resources can be categorized into two primary aspects. Firstly, climate change-induced variations in hydrological conditions directly affect the operation and efficiency of hydropower plants. Fluctuations in precipitation and water availability amplify operational uncertainty, thereby undermining electricity generation and the stability of energy supplies (van Vliet et al., 2016). These impacts are evident in the hydrological cycle, where changes in precipitation frequency, timing, spatial distribution, and intensity exacerbate unpredictability. Secondly, traditional hydropower resource planning and management frameworks require reassessment and adaptation in the context of altered climate conditions. Conventional planning approaches, which often rely on historical hydrological data, may no longer provide reliable guidance under current and projected climatic shifts. To address these challenges, it is imperative to adopt advanced and integrative scientific methodologies alongside cutting-edge technological tools to comprehensively analyze water resource supply and demand dynamics. Such approaches will enable the development of more adaptive and sustainable hydropower planning and management strategies (Holanda et al., 2017; Ullah et al., 2019; Yang et al., 2020).

Amid the context of climate change, numerous scholars, both domestically and internationally, have conducted in-depth investigations into future changes in hydropower resources. Chuphal and Mishra (2023) employed hydrological models to explore runoff variations to major dams in India under three shared socio-economic pathway (SSP) scenarios: SSP1-2.6, SSP2-4.5, and SSP3-7.0. Their findings revealed that trends in Gross Hydropower Potential (GHP) aligned closely with changes in runoff patterns. Similarly, Dallison and Patil (2023) utilized the EXP–HYDRO hydrological model to simulate flow changes across 585 river basins in the UK and Ireland under the SSP5-8.5 scenario. They analyzed the implications of these changes for hydropower extraction in 178 watersheds, providing insights into regional hydropower resource dynamics. In China, Liu and Xu (2022) conducted a comprehensive estimation and uncertainty analysis of the country's total and developed GHP. Their study integrated eight global hydrological models driven by five atmospheric models, using climate data under two representative concentration pathway (RCP) scenarios (RCP2.6 and RCP8.5) (Liu et al., 2016). Similarly, by combining ten climate models with hydrological models (Variable Infiltration Capacity (VIC) and Coupled Routing and Excess STorage (CREST)), Zhao et al. (2021) projected changes in runoff and hydropower resources in the Yalong River, China. Their results indicated that, compared to the baseline period (1996–2012), dry season runoff in the basin is expected to increase, rainy season runoff is expected to decrease, daily runoff variability is expected to decline, and future electricity generation in the Three Gorges Reservoir Area is expected to follow the projected trends in runoff changes. These studies collectively enhance our understanding of how climate change influences global hydropower resources, providing critical insights for the adaptation and sustainable management of hydropower systems in a warming world.

Over the past two decades, the academic community has shown considerable interest in the changing flow of the Kaidu River, China and the water volume of its terminal lake, Bosten Lake. Tuoheti and Aji (2022) demonstrated that various climatic variables influence the runoff of the Kaidu River, with annual average temperature exerting the most significant effect, followed by

annual precipitation and annual evaporation. Chen et al. (2013) analyzed the hydrological sensitivity of the runoff of the Kaidu River from 1994 to 2009, concluding that the river's runoff responded more strongly to climate change than to human activities. Fang et al. (2023) employed the extended Soil and Water Assessment Tool (SWAT) model (SWAT–Glacier) to project future runoff changes in four rivers within the Tarim Basin, China. Their findings indicated a slight decreasing trend in the runoff of the Kaidu River, with projected reductions of approximately 2.31% and 7.80% by 2035 under RCP4.5 and RCP8.5 scenarios, respectively. These studies collectively highlight the pronounced sensitivity of rivers and lakes in arid regions to climate change. Notably, the impacts of changes in runoff on hydropower resources have yet to receive widespread attention—a critical gap in ensuring future hydropower security and sustainable development in the region. To address this, the present study focused on the Kaidu River, often referred to as the "Little Three Gorges of Xinjiang", to explore the impacts of climate change on future runoff and hydropower resources in the basin. First, we processed and analyzed the Coupled Model Intercomparison Project Phase 6 (CMIP6) Global Climate Model (GCM) data using Delta downscaling bias correction and multi-model equal-weight ensemble averaging to investigate the spatiotemporal evolution of precipitation and temperature in the Kaidu River Basin from 1980 to 2070. Second, a hydrological model (VIC) integrated with a glacier module (VIC–Glacier) was developed to analyze runoff responses to climate change. Finally, based on the simulated runoff, changes in GHP and electricity generation were estimated under four SSP scenarios (SSP1-2.6, SSP2-4.5, SSP3-7.0, and SSP5-8.5). The findings of this study will provide a scientific basis for decision-making in water resource and hydropower planning, operation, and management in the Kaidu River Basin.

2 Materials and methods

2.1 Study area

The Kaidu River originates in the central Tianshan Mountains, located in the Bayingol Mongolian Autonomous Prefecture of Xinjiang Uygur Autonomous Region, China. It flows through the large and small Yulduz basins, traverses canyons, passes through the Yanqi Basin, and ultimately discharges into the Bosten Lake, serving as a major source of replenishment for the lake (Zhang et al., 2007). As a typical inland river in arid regions, the Kaidu River experiences concentrated precipitation primarily between June and September, with low annual precipitation and high evaporation. Annual precipitation ranges from 300.00 to 600.00 mm, while annual evaporation ranges from 600.00 to 1100.00 mm. The river's water resources are predominantly derived from precipitation, glacier melt, and snowmelt, resulting in an average annual runoff volume of approximately 34.41×10^8 m^3, and 56.12% of the runoff occurs between June and September. Dashankou, the sole mountain pass along the Kaidu River, divides the entire basin into an upstream mountainous area and a downstream plain area (Chen et al., 2013). The study area covers the Kaidu River Basin above the Dashankou Hydrological Station that extends approximately 610 km, encompassing a catchment area of 1.83×10^4 km^2 (Fig. 1). This region features complex mountainous terrain with an average elevation of 2998 m, sloping gradually from northwest to southeast. The narrow riverbed and rapid river flow create substantial hydropower potential, making this area the primary location for hydropower stations within the basin (Fan et al., 2021). Among these hydropower projects, the Dashankou Hydropower Station, situated 1 km upstream from the canyon's outlet, stands out as one of the larger hydropower facilities in Xinjiang. Completed in 1992, the station has an installed capacity of 80 MW and a designed annual electricity generation of 3.10×10^8 kWh. In addition to electricity generation, the station provides other critical benefits, such as flood control.

2.2 Data sources

2.2.1 Meteorological data

This study utilized the CN05.1 meteorological dataset (1980–2016) provided by the Climate

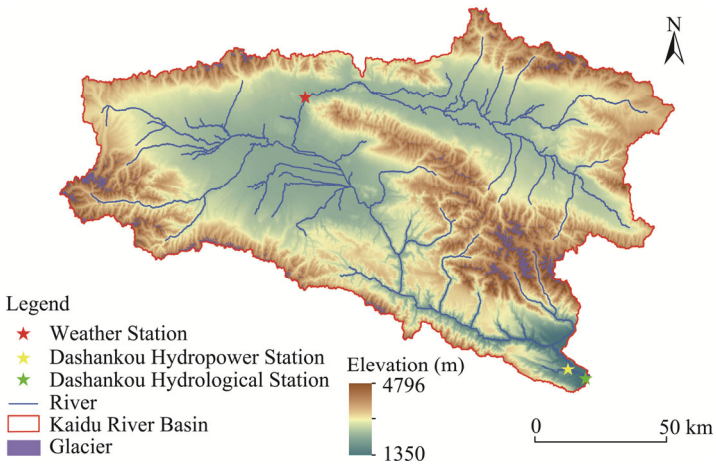

Fig. 1 Overview of river network and glacier distribution in the Kaidu River Basin. Elevation data are sourced from the Geospatial Data Cloud (https://www.gscloud.cn/), and glacier data are sourced from the National Cryosphere Desert Data Center (http://www.ncdc.ac.cn/portal/).

Change Research Center of the Chinese Academy of Sciences. This dataset was generated through the interpolation of climate and anomaly fields integrating observations from over 2400 meteorological stations across China, and has a spatial resolution of 0.25°×0.25°. Five variables including precipitation (mm), mean temperature (°C), maximum temperature (°C), minimum temperature (°C), and wind speed (m/s) were selected as the data foundation for the research analysis (Wu and Gao, 2013). Building upon previous research, five CMIP6 GCMs (EC-Earth3, EC-Earth3-Veg, EC-Earth3-Veg-LR, INM-CM5-0, and IPSL-CM6A-LR) suitable for the arid regions of China were selected to simulate climatic variables in the study area for the period 1980–2070 (Liu et al., 2022). Projections of climatic variables in this study (2017–2070) were based on four SSP scenarios: SSP1-2.6, a low-emission scenario under sustainable green development; SSP2-4.5, a medium-emission scenario reflecting a middle-of-the-road pathway; SSP3-7.0, a medium-high-emission scenario characterized by regional rivalry and fragmented approaches; and SSP5-8.5, a high-emission scenario dominated by fossil fuel-intensive development.

2.2.2 Hydrological data

Daily observed runoff data (m^3/s) from the Dashankou Hydrological Station (1985–2016), provided by the Hydrology Bureau of Xinjiang Uygur Autonomous Region, were utilized to evaluate the simulation performance of the VIC–Glacier model. Additionally, observed data, including water head (m) and electricity generation (kWh) from 2001 to 2016 at the Dashankou Hydropower Station, were employed to estimate the GHP (MW) and electricity generation for both the baseline period (1985–2016) and future period (2017–2070). These data were sourced from the Midstream Management Station of the Bayingol Mongolian Autonomous Prefecture, under the Xinjiang Tarim River Basin Authority.

2.2.3 Ancillary data

The ancillary data used in the models included digital elevation model (DEM) data (https://www.gscloud.cn/search), soil texture data (https://www.fao.org/home/en), vegetation type data (https://www.landcover.org/data/landcover/data.shtml), and glacier data (http://www.ncdc.ac.cn/portal/).

2.3 Methods

2.3.1 Downscaling bias correction

Delta downscaling bias correction is a straightforward and commonly used technique in climate modeling (Xavier et al., 2022). It involves overlaying the variation characteristics of simulated climatic variables onto observed climate data in the baseline period. This process reconstructs

climate scenarios by applying the simulated changes (such as the absolute increase in temperature or the relative change in precipitation) to the data series of climatic variables measured during the baseline period. The approach to adjusting precipitation and temperature differs. Specifically, for precipitation, the relative change in gridded precipitation from GCMs is applied; whereas for temperature, the absolute change in gridded temperature from GCMs is used (Luo et al., 2019). The specific formulas employed to implement these adjustments are as follows:

$$T_f = T_o + (T_{Mf} - T_{Mo}), \tag{1}$$

$$P_f = P_o \times (P_{Mf} / P_{Mo}), \tag{2}$$

where T_f represents the gridded temperature data reconstructed using the Delta downscaling bias correction method (°C); T_o represents the multi-year average of the observed temperature data during the baseline period (°C); T_{Mf} represents the simulated gridded temperature data for the baseline period (°C); T_{Mo} represents the multi-year average of the simulated gridded temperature data during the baseline period (°C); P_f represents the gridded precipitation data reconstructed using the Delta downscaling bias correction method (mm); P_o represents the multi-year average of the observed precipitation data during the baseline period (mm); P_{Mf} represents the simulated gridded precipitation data for the baseline period (mm); and P_{Mo} represents the multi-year average of the simulated gridded precipitation data during the baseline period (mm).

After Delta downscaling bias correction for climatic variables in CMIP6 GCMs, this study used multi-model equal-weight ensemble averaging to investigate the spatiotemporal evolution of precipitation and temperature in the Kaidu River Basin from 1980 to 2070.

2.3.2 VIC model

The VIC model, introduced in 1994, is a large-scale land surface hydrological model designed to simulate both water and energy balances between the land and the atmosphere (Wood et al., 1992). This model places particular emphasis on the simulation of thermal processes, addressing a key limitation of traditional hydrological models. The main components of the VIC model include evapotranspiration, runoff generation, and streamflow routing (Lohmann et al., 1998; Asgari et al., 2022). The model divides the watershed into multiple grid cells, calculates runoff generation at each grid, and routes the output data into streamflow processes at the watershed outlet using the routing module (Castaneda-Gonzalez et al., 2023). The input parameters required for the VIC hydrological model include soil data, vegetation type data, meteorological forcing data, flow direction data, watershed characteristic data, and global parameter files. After calibration, the model incorporates the multi-model ensemble of climatic variables—such as precipitation, maximum and minimum temperatures, and wind speed—as meteorological inputs to predict future runoff changes.

To enhance the visualization of simulated runoff across dry and wet seasons, daily runoff data were aggregated into monthly scales. The period from 1980 to 1984 was designated as a model warm-up phase to minimize the impact of initial conditions on simulation outcomes. The model calibration period, spanning from 1985 to 2000, was employed to optimize model parameters and improve simulation accuracy. Subsequently, the years 2001 to 2016 were used as the validation period to assess the model's performance on independent data. Three key performance metrics—namely the Nash-Sutcliffe efficiency (NSE), relative error (RE; %), and correlation coefficient (CC)—were utilized to evaluate the model's simulation performance. The formulas for these metrics are as follows:

$$\mathrm{NSE} = 1 - \frac{\sum_{i=1}^{n} (Q_{\mathrm{sim},i} - Q_{\mathrm{obs},i})^2}{\sum_{i=1}^{n} (Q_{\mathrm{obs},i} - \overline{Q}_{\mathrm{obs}})^2}, \tag{3}$$

$$\mathrm{RE} = \frac{\sum_{i=1}^{n} (Q_{\mathrm{sim},i} - Q_{\mathrm{obs},i})}{\sum_{i=1}^{n} Q_{\mathrm{obs},i}} \times 100\%, \tag{4}$$

$$\mathrm{CC}=\frac{\sum_{i=1}^{n}(Q_{\mathrm{sim},i}-\overline{Q}_{\mathrm{sim}})(Q_{\mathrm{obs},i}-\overline{Q}_{\mathrm{obs}})}{\sqrt{\sum_{i=1}^{n}(Q_{\mathrm{sim},i}-\overline{Q}_{\mathrm{sim}})^2\sum_{i=1}^{n}(Q_{\mathrm{obs},i}-\overline{Q}_{\mathrm{obs}})^2}}, \tag{5}$$

where n is the total number of observations; $Q_{\mathrm{sim},i}$ and $Q_{\mathrm{obs},i}$ represent the simulated runoff (m^3/s) and observed runoff (m^3/s) at time step i, respectively; and $\overline{Q}_{\mathrm{sim}}$ and $\overline{Q}_{\mathrm{obs}}$ represent the average values of simulated runoff (m^3/s) and observed runoff (m^3/s), respectively.

2.3.3 VIC–Glacier model

The VIC model does not include a glacier melt module in its standard configuration. To address this limitation, this study coupled the VIC model with a daily glacier melt algorithm, referred to as the VIC–Glacier model (Hock, 2003), to simulate hydrological processes in both glaciated and non-glaciated areas within the study area. The VIC–Glacier model has been successfully validated in various river basins (Zhang et al., 2013; Su et al., 2016; Kan et al., 2018). The input data for the enhanced model included daily climatic variables (such as precipitation, maximum and minimum temperatures, and wind speed), vegetation type, soil texture, and glacier area percentage. To account for terrain influences, glaciated areas were divided into 100 m elevation bands, allowing for a more precise estimation of glacier meltwater than using a uniform temperature across the entire glacier within each modeling grid.

The total runoff from each grid originated from both glaciated and non-glaciated areas, and the formulas are as follows:

$$R=f\times R_{\mathrm{melt}}+(1-f)\times R_{\mathrm{VIC}}, \tag{6}$$

$$R_{\mathrm{melt}}=M_1+M_2+\cdots+M_j, \tag{7}$$

$$M_j=\begin{cases}\mathrm{DDF}\times(T-T_{\mathrm{base}}) & \text{if } T>T_{\mathrm{base}}\\ 0 & \text{if } T\le T_{\mathrm{base}}\end{cases}, \tag{8}$$

where R is the total runoff depth of the grid (mm); f represents the percentage of the glaciated areas (%); R_{melt} is the runoff depth from the glaciated areas (mm); R_{VIC} is the runoff depth from the non-glaciated areas (mm); M_j is the meltwater from elevation band j (mm); DDF is the degree–day factor for glacier or snow melt (mm/(°C•d)); T the daily average temperature above the glacier surface adjusted by the temperature lapse rate (°C); and T_{base} is the temperature threshold between rain and snow (°C), typically with temperatures above zero classified as rainfall and below zero as snowfall.

2.3.4 Estimation of GHP

The formula used to estimate the GHP (MW) is as follows (Chuphal and Mishra, 2023):

$$\mathrm{GHP}=Q\times h\times g\times\rho\times10^{-6}, \tag{9}$$

where Q denotes the runoff (m^3/s); h represents the water head (m); g stands for the gravitational acceleration (9.80 m/s^2); and ρ is the density of water (1000 kg/m^3).

2.3.5 Estimation of CO_2 emission reductions

Given that CO_2 comprises approximately 90.00% of greenhouse gases emitted from human activities, this study primarily focused on CO_2 emissions. It is assumed that the reduction in CO_2 emissions equals to the amount of CO_2 emitted by coal-fired power generation minus the CO_2 emitted by hydropower generation. The difference between these two values represents the role of hydropower in reducing CO_2 emissions. The formula is as follows:

$$V=(\alpha-\beta)x, \tag{10}$$

where V represents the CO_2 emission reduction by hydropower generation (t); α represents the constant of CO_2 emission by coal-fired power generation at 9.65×10^{-4} t/kWh (IPCC, 2023); β represents the constant of CO_2 emission by hydropower generation at 1.90×10^{-5} t/kWh (IPCC, 2015); and x represents the electricity generated (kWh).

3 Results

3.1 Spatiotemporal evolution characteristics of precipitation and temperature

3.1.1 Temporal variability of precipitation and temperature

Compared to the baseline period (1980–2016), all four SSP scenarios exhibit a fluctuating increasing trend in precipitation (Fig. 2a). The SSP2-4.5 scenario predicts the largest increase rate, reaching 2.51 mm/10a, while the SSP3-7.0 scenario predicts the smallest increase rate, at only 0.25 mm/10a. The trends for the three temperature variables—mean, maximum, and minimum temperatures—are consistent, with the rate of warming accelerating as greenhouse gas emission intensifies. The high emission scenario (SSP5-8.5) predicts a significantly faster warming rate compared to the other three scenarios (Fig. 2b–d). Under the low emission scenario (SSP1-2.6), mean temperature increases by approximately 0.20°C/10a, maximum temperature increases by about 0.21°C/10a, and minimum temperature increases by around 0.22°C/10a. Conversely, under the SSP5-8.5 scenario, mean temperature rises by approximately 0.70°C/10a, maximum temperature rises by 0.68°C/10a, and minimum temperature rises by 0.74°C/10a. From a temporal perspective, between 2017 and 2040, the warming rates for the three temperature variables across all four SSP scenarios remain similar. However, during the mid-term period from 2041 to 2070, as greenhouse gas emission increases, temperature differences among the scenarios become more pronounced. Notably, under the SSP5-8.5 scenario, the warming rates for the three temperature variables are more than double those observed under the moderate emission scenario (SSP2-4.5). This suggests that the probability of extreme climate events may significantly increase under high emission scenarios.

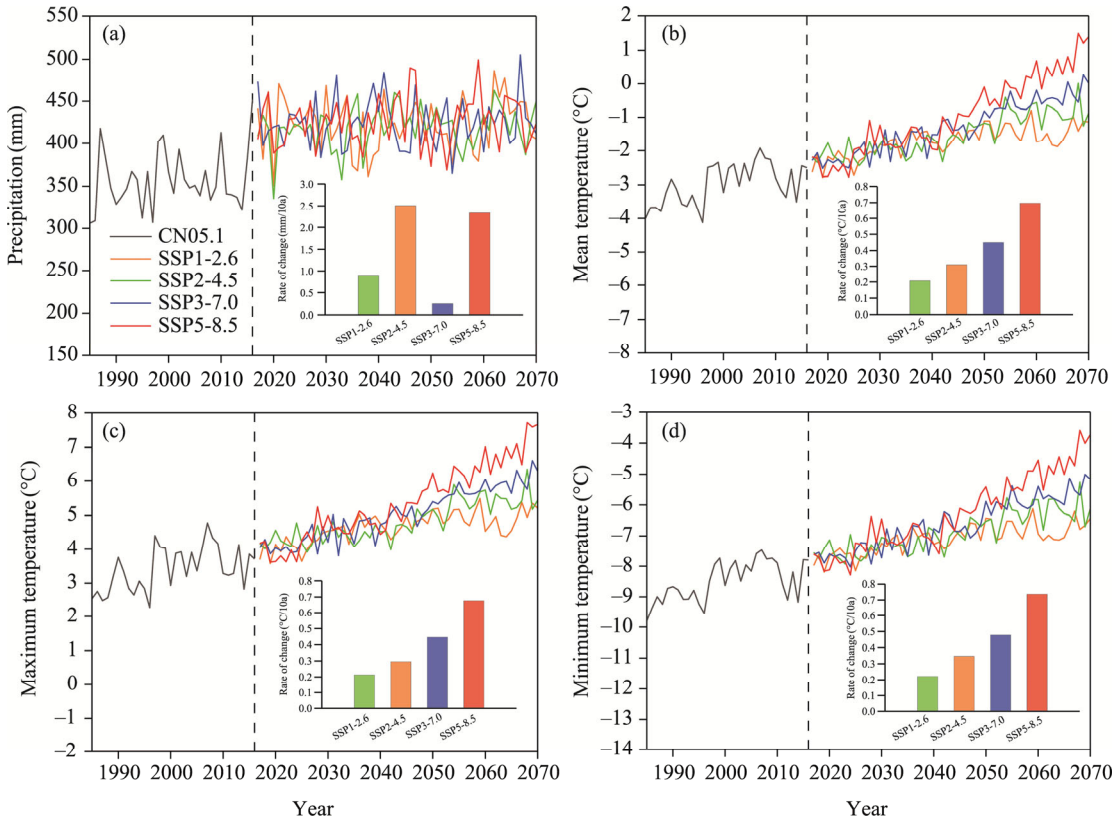

Fig. 2 Temporal variations in annual precipitation (a), mean temperature (b), maximum temperature (c), and minimum temperature (d) of the Kaidu River Basin during the baseline period (1980–2016) and future period (2017–2070) under four shared socio-economic pathway (SSP) scenarios (SSP1-2.6, SSP2-4.5, SSP3-7.0, and SSP5-8.5). The CN05.1 data were used during the baseline period.

3.1.2 Spatial variability of precipitation and temperature

Under the four SSP scenarios, the spatial distribution of precipitation remains relatively consistent, exhibiting a gradual increase from southeast to northwest (Fig. 3). The multi-year average precipitation ranges from 170 to 660 mm, with high-precipitation areas primarily concentrated in the northwestern and northeastern parts of the study area, while the southern mountains receive significantly less precipitation. The multi-year average of mean temperature ranges from –6.5°C to 4.5°C. Although spatial variability exists among different scenarios, mean temperature shows consistent general distribution pattern that decreases from southwest to northeast. Warming intensifies with increasing greenhouse gas emissions, reaching its peak under the SSP5-8.5 scenario. The multi-year average maximum temperature ranges from –0.4°C to 11.5°C. Under the SSP1-2.6 scenario, the distribution of multi-year average maximum temperature closely resembles that observed during the baseline period, whereas the other scenarios demonstrate progressively greater warming as greenhouse gas emission intensifies. The multi-year average minimum temperature ranges from –11.0°C to –3.0°C, with higher temperature areas mainly concentrated in the northwest and southeast of the study area, and lower temperatures prevailing in the mountainous regions in the northeast. Among all four SSP scenarios, the SSP5-8.5 scenario predicts the most pronounced warming changes.

The projected precipitation exhibits an overall increasing trend across the four SSP scenarios, with spatial variability in the magnitude of these increases (Fig. 4). Under the SSP3-7.0 scenario,

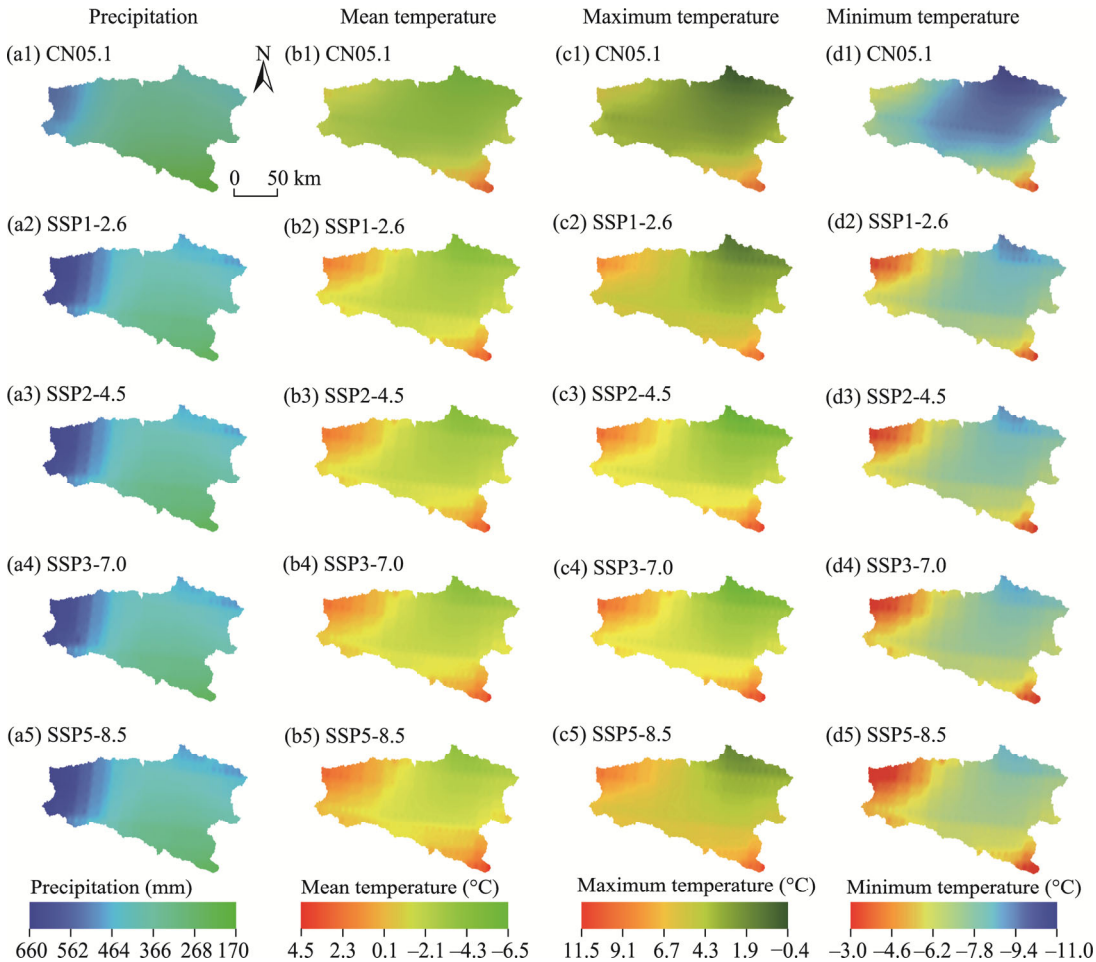

Fig. 3 Spatial distributions of multi-year average precipitation (a1–a5), mean temperature (b1–b5), maximum temperature (c1–c5), and minimum temperature (d1–d5) during the baseline period (1980–2016) and future period (2017–2070) under the four SSP scenarios (SSP1-2.6, SSP2-4.5, SSP3-7.0, and SSP5-8.5)

the most pronounced increase in precipitation is expected in the northwestern region (6.81 mm/10a), while the central region may experience the largest decrease (–1.91 mm/10a). In contrast, the SSP2-4.5 scenario predicts an increase in precipitation across the entire basin, with varying magnitudes ranging from 0.82 to 4.82 mm/10a in different regions. All three temperature variables—mean, maximum, and minimum temperatures—are expected to demonstrate warming trends under the four scenarios, with varying regional intensities. The warming rates for these temperature variables are projected to become more pronounced under higher emission scenarios. For mean temperature, the western region is anticipated to experience greater warming than the eastern region, with the most significant increase under the SSP5-8.5 scenario, reaching up to 0.72°C/10a. Notable spatial differences in the warming rate of maximum temperature are observed among the four SSP scenarios. The SSP1-2.6 scenario predicts the largest increase in maximum temperature in the northern region (0.22°C/10a), while the SSP3-7.0 scenario predicts the largest increase in the central and eastern regions (0.45°C/10a). For minimum temperature, the spatial distribution of warming rates is expected to be consistent across scenarios, with greater warming projected in the western region compared to the eastern region. The SSP5-8.5 scenario predicts the most notable increase in minimum temperature, ranging from 0.72°C/10a to 0.78°C/10a. Overall, a strengthening warming trend is expected across the study area in the future, with both precipitation and temperature changes displaying significant spatial variability.

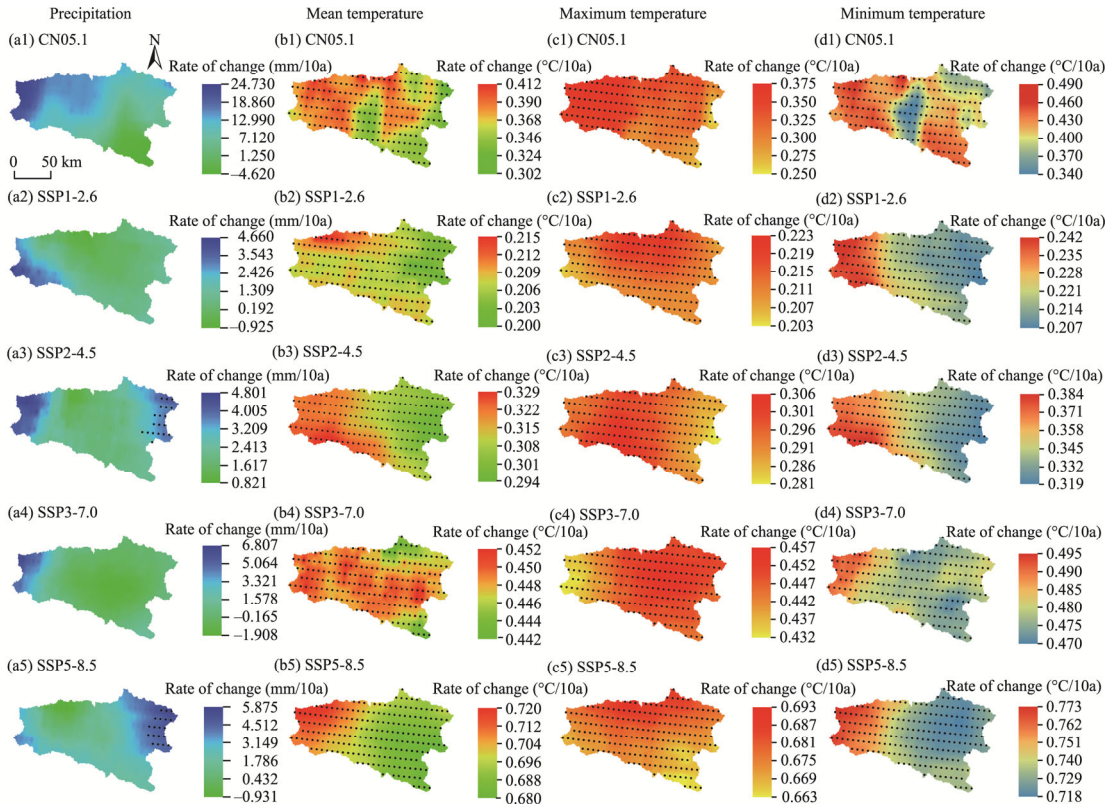

Fig. 4 Spatial distributions of trends in annual precipitation (a1–a5), mean temperature (b1–b5), maximum temperature (c1–c5), and minimum temperature (d1–d5) for the baseline period (1980–2016) and future period (2017–2070) under the four SSP scenarios (SSP1-2.6, SSP2-4.5, SSP3-7.0, and SSP5-8.5). Regions marked with dots indicate statistically significant trends in these variables (P<0.05).

3.2 Runoff simulation and projection

3.2.1 Historical runoff simulation using the VIC and VIC–Glacier models

Figure 5 compares observed and simulated runoff during the calibration and validation periods using the VIC and VIC–Glacier models. The VIC–Glacier model demonstrated superior

performance, particularly during peak- and low-flow periods. In the Kaidu River Basin, water resources originate from a combination of precipitation, glacier melt, and snowpack inputs. Glaciers in the mountainous upstream areas indirectly contribute to runoff through their storage and gradual release of meltwater. The traditional VIC model, which lacks a glacier melt component, introduces biases in runoff simulations, particularly in high-altitude regions where glaciers significantly influence peak flow periods. In contrast, the VIC–Glacier model addressed this limitation by incorporating terrain effects and dividing glacierized areas into 100 m elevation bands. This approach enables a more accurate estimation of glacier meltwater, resolving the issue of uniform glacier temperatures within modeling grids. As a result, the VIC–Glacier model can effectively capture peak flows associated with meltwater runoff, leading to more precise simulations of runoff changes in the basin (Fig. 6). Consequently, the VIC–Glacier model is more reliable for projecting future runoff, especially in glacier-dominated watersheds.

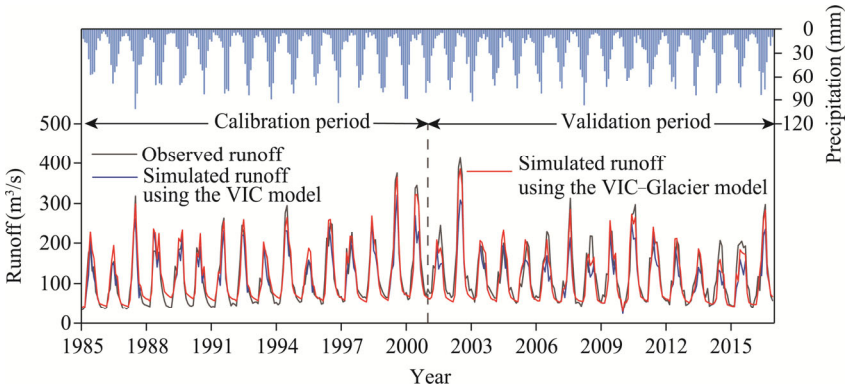

Fig. 5 Comparison of observed and simulated runoff using both the VIC model and VIC–Glacier model during the calibration (1985–2000) and validation (2001–2016) periods. VIC, Variable Infiltration Capacity; VIC–Glacier, the VIC model coupled with a glacier module.

3.2.2 Future runoff projection using the VIC–Glacier model

Future runoff projected in the VIC–Glacier model exhibits a fluctuating downward trend, with obvious differences among the four scenarios (Fig. 7). The higher emission scenarios (SSP3-7.0 and SSP5-8.5) project a more pronounced decline rate of runoff per decade, at 7.04 and 7.20 m^3/s, respectively. These rates are significantly higher than those under the lower emission scenarios (SSP1-2.6 and SSP2-4.5), with decline rates of 3.09 and 3.42 m^3/s per decade, respectively. Runoff under the SSP5-8.5 scenario not only exhibits greater variability but also the most marked declining trend, potentially linked to its higher projected greenhouse gas emissions, which may intensify climate change and increase the frequency of extreme climate events, adversely affecting runoff. Notably, specific years, such as 2045 and 2046 under the SSP5-8.5 scenario and 2045 under the SSP1-2.6 scenario, show significant peaks and troughs in runoff, possibly indicating extreme climate events like droughts and floods. During 2020–2030, all scenarios predict significant variability in runoff, likely reflecting natural climate fluctuations and the short-term impacts of socio-economic factors.

Runoff exhibits pronounced seasonal variations across the four scenarios (Fig. 7a). Peak runoff occurs in July, with values of 178.06, 180.36, 185.79, and 185.72 m^3/s under the SSP1-2.6, SSP2-4.5, SSP3-7.0, and SSP5-8.5 scenarios, respectively. In contrast, the lowest runoff occurs in early March, with values of 45.80, 45.70, 47.32, and 48.36 m^3/s under the SSP1-2.6, SSP2-4.5, SSP3-7.0, and SSP5-8.5 scenarios, respectively. The summer peak may be primarily driven by increased precipitation and higher temperatures, which enhance glacier meltwater and surface runoff, particularly under higher emission scenarios (SSP3-7.0 and SSP5-8.5). Conversely, spring represents the low-flow period due to reduced precipitation and limited snowmelt contribution.

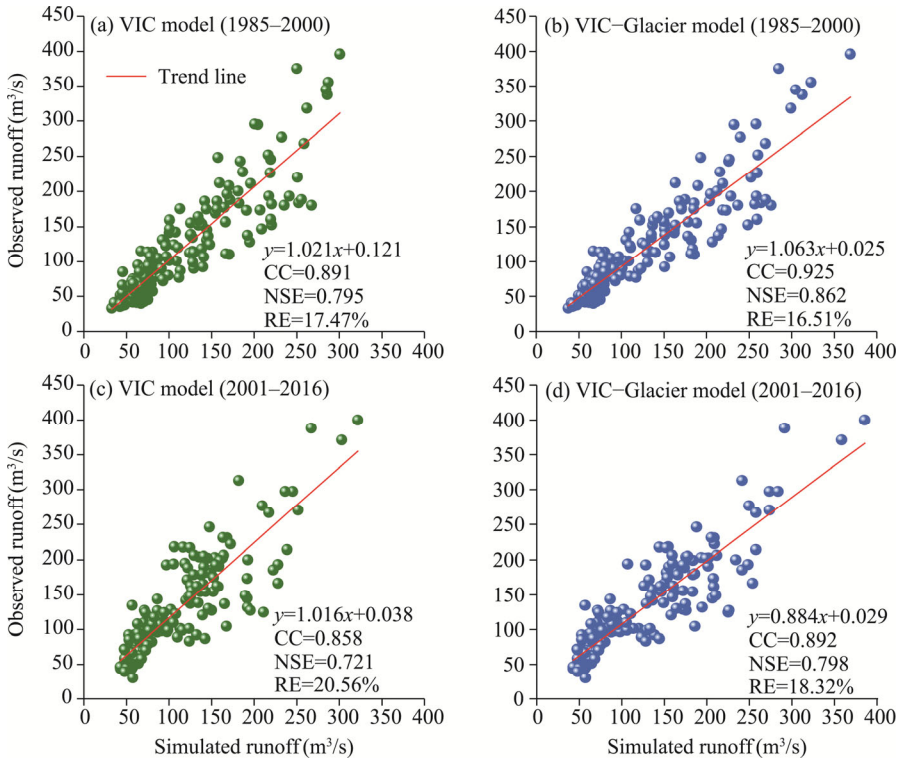

Fig. 6 Scatter plots showing the runoff simulation performance of the VIC (a and c) and VIC–Glacier (b and d) models during the calibration (1985–2000) and validation (2001–2016) periods. CC, correlation coefficient; NSE, Nash-Sutcliffe efficiency; RE, relative error.

3.3 Estimation of hydropower resources and CO_2 emission reductions

3.3.1 Estimated GHP under the SSP1-2.6, SSP2-4.5, SSP3-7.0, and SSP5-8.5 scenarios

Under the four SSP scenarios, GHP exhibits a fluctuating downward trend (Fig. 8a). Specifically, under the SSP1-2.6 scenario, GHP declines at a rate of 507.74 MW/10a. In contrast, under the SSP2-4.5 scenario, GHP shows greater variability, changing at a rate of 563.33 MW/10a, with a stable minor decrease around the year 2045 (372.31 MW/10a), potentially reflecting mid-term climate impacts. GHP under both the SSP3-7.0 and SSP5-8.5 scenarios demonstrates significant variability throughout the period 2017–2070, with decline rates of 1158.42 and 1184.53 MW/10a, respectively. GHP under the SSP5-8.5 scenario shows pronounced declines during 2020–2040 (1032.61 MW/10a) and 2045–2060 (2052.34 MW/10a), highlighting the challenges faced by GHP under high greenhouse gas emissions and unsustainable development pathways.

GHP under all four SSP scenarios exhibits significant seasonal variations, as shown in Figure 8b. Specifically, GHP peaks during the summer months, exceeding the annual average by about 92.12% to 96.31%. GHP under the SSP5-8.5 scenario demonstrates a more pronounced peak in summer, likely due to increased rainfall, glacier melt, and snowmelt contributing to higher runoff. Conversely, at the beginning of spring (March), GHP drops to its lowest, about 50.05% below the annual average, indicating a period of water scarcity and correspondingly lower GHP. A shift in the peak period of GHP from June to July can be observed across all four SSP scenarios. For SSP1-2.6, the peak occurs in June during 2021–2030; for SSP2-4.5, it shifts to June during the periods of 2051–2060 and 2061–2070; for SSP3-7.0, it occurs in June during 2061–2070; for SSP5-8.5, it occurs in June during the periods of 2041–2050, 2051–2060, and 2061–2070. The frequent early peaks under the SSP5-8.5 scenario highlight the need to closely monitor the seasonal variability of GHP, especially under high emission scenarios.

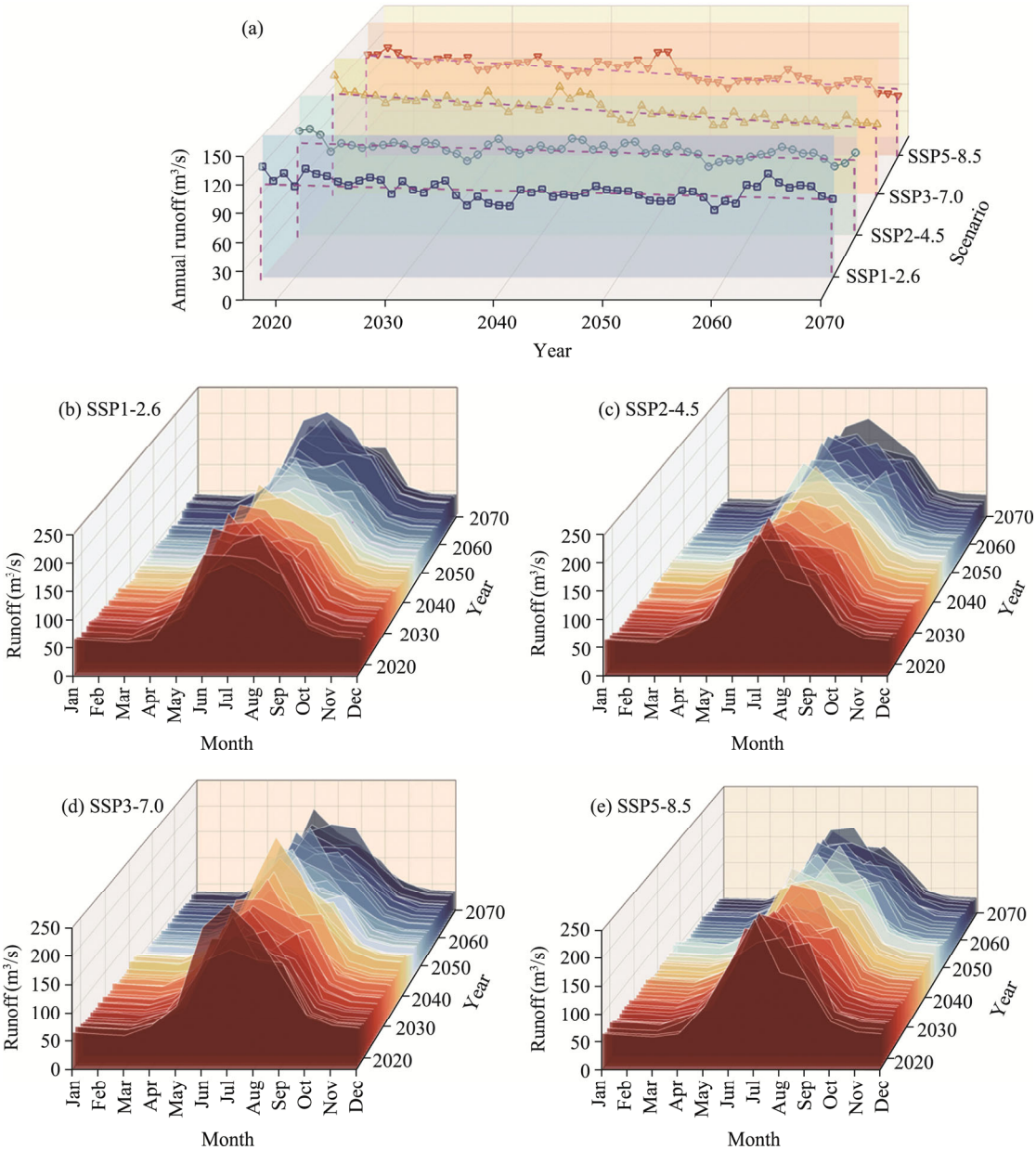

Fig. 7 Variations in annual runoff (a) and monthly runoff (b–e) from 2017 to 2070 under the SSP1-2.6, SSP2-4.5, SSP3-7.0, and SSP5-8.5 scenarios

3.3.2 Estimated electricity generation under the SSP1-2.6, SSP2-4.5, SSP3-7.0, and SSP5-8.5 scenarios

Figure 9 depicts the annual variations in electricity generation and runoff. Notable differences emerge in the trends of electricity generation across all four SSP scenarios. Under the lower emission scenarios (SSP1-2.6 and SSP2-4.5), the slope of the fitted curve for annual electricity generation is relatively small, indicating greater stability in electricity production over time. In contrast, the annual electricity generation under the higher emission scenarios (SSP3-7.0 and SSP5-8.5) exhibit a more pronounced downward trend, reflecting increased instability in electricity generation. These results align with the observed variations in runoff. As greenhouse gas emission increases, both runoff and hydropower generation display accelerated rates of decline, underscoring the sensitivity of hydropower systems to changes in climate forcing.

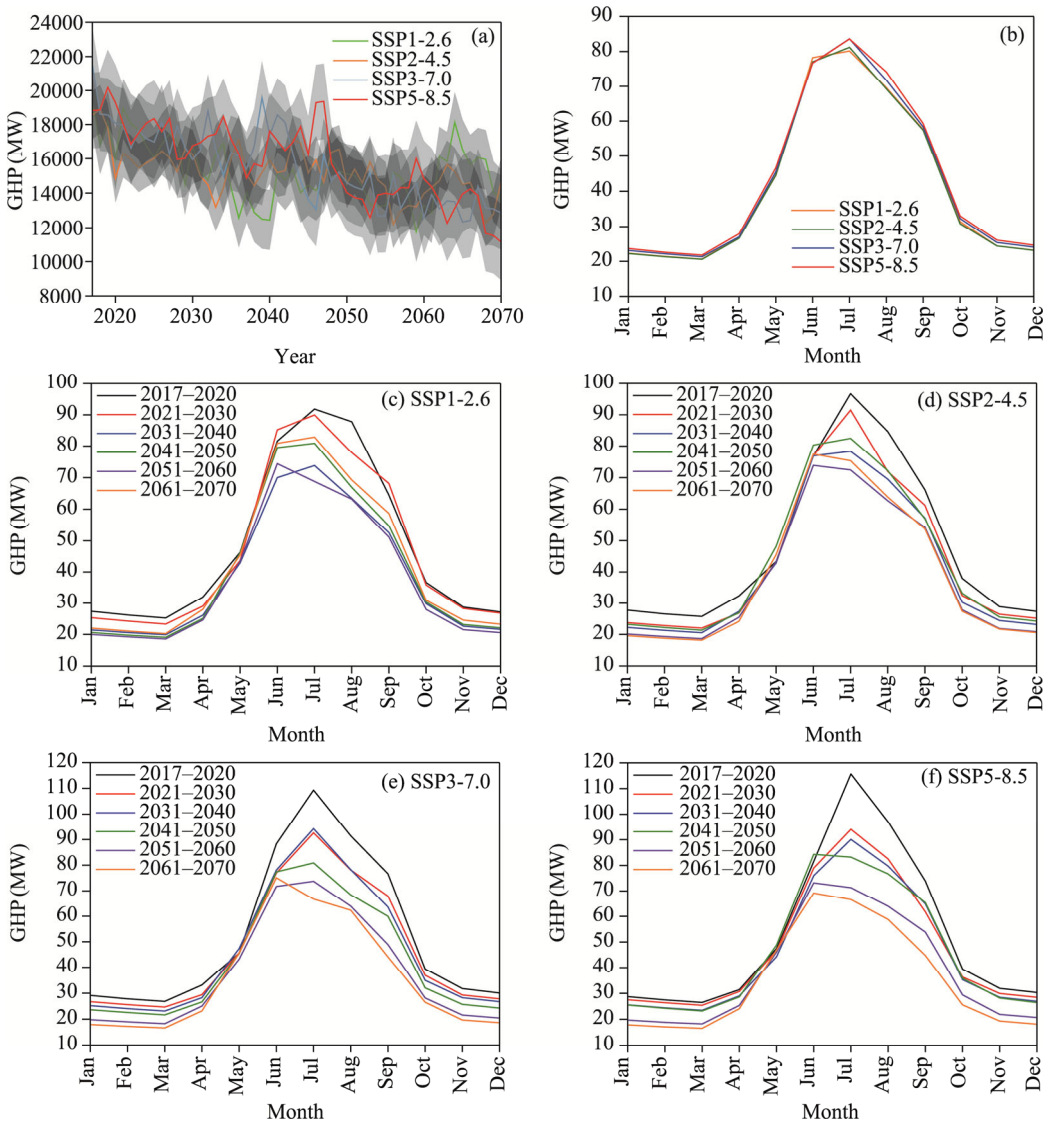

Fig. 8 Variations in annual total GHP (a), monthly average GHP (b), and segmented monthly average GHP (c–f) during 2017–2070 under the four SSP scenarios (SSP1-2.6, SSP2-4.5, SSP3-7.0, and SSP5-8.5)

Under the SSP1-2.6, SSP2-4.5, SSP3-7.0, and SSP5-8.5 scenarios, the average annual electricity generation of the reservoirs from 2017 to 2070 is approximately 3.12×10^8, 3.11×10^8, 3.19×10^8, and 3.25×10^8 kWh, respectively, with the highest value observed under the SSP5-8.5 scenario. Observing by periods, the average annual electricity generation during 2017–2040 under the SSP1-2.6, SSP2-4.5, SSP3-7.0, and SSP5-8.5 scenarios is 3.26×10^8, 3.25×10^8, 3.55×10^8, and 3.56×10^8 kWh, respectively. This indicates an increasing trend in electricity generation before the 2040s, with relative rates of change compared to the overall period being 4.31%, 4.32%, 11.27%, and 9.76%, respectively. During 2041–2070, the average annual electricity generation under the SSP1-2.6, SSP2-4.5, SSP3-7.0, and SSP5-8.5 scenarios is 3.02×10^8, 3.01×10^8, 2.90×10^8, and 2.99×10^8 kWh, respectively. The relative rates of change compared to the overall period are –3.44%, –3.45%, –9.01%, and –7.81%, respectively. The most significant decline is observed under the SSP3-7.0 scenario during this period. The decrease in generation during this phase is a critical signal for the hydropower industry, necessitating attention from hydroelectric-related sectors to the impact of climate change on hydropower generation.

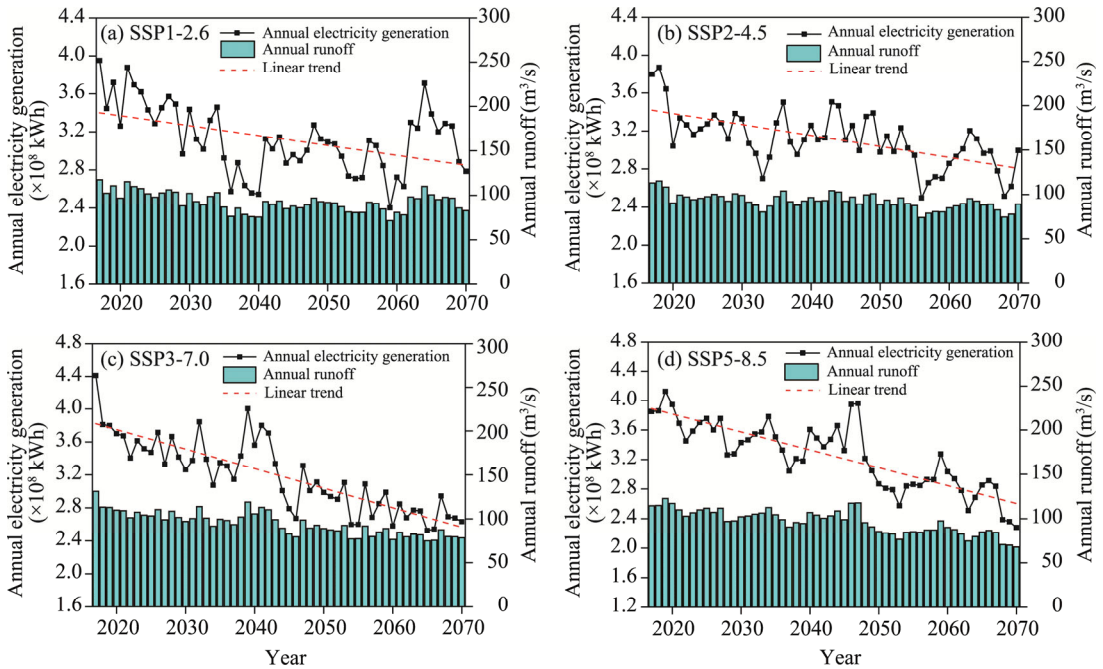

Fig. 9 Variations in electricity generation and runoff from 2017 to 2070 under the SSP1-2.6 (a), SSP2-4.5 (b), SSP3-7.0 (c), and SSP5-8.5 (d) scenarios

3.3.3 Estimated CO_2 emission reductions under SSP1-2.6, SSP2-4.5, SSP3-7.0, and SSP5-8.5 scenarios

The CO_2 emission reductions under the four SSP scenarios all show a decreasing trend, though there are significant differences among them (Fig. 10). Before 2050, higher CO_2 emission reductions can be observed under SSP3-7.0 and SSP5-8.5 scenarios compared to the lower emission scenarios (SSP1-2.6 and SSP2-4.5). However, after 2050, the decreasing trend of CO_2 emission reduction across all four SSP scenarios begin to slow and converge. Beyond 2060, the lower emission scenarios (SSP1-2.6 and SSP2-4.5) surpass the higher emission scenarios (SSP3-7.0 and SSP5-8.5) in terms of CO_2 emission reduction. Specifically, the annual average CO_2 emission reductions under SSP1-2.6, SSP2-4.5, SSP3-7.0, and SSP5-8.5 scenarios are 2.60×10^5, 2.59×10^5, 2.65×10^5, and 2.70×10^5 t, respectively.

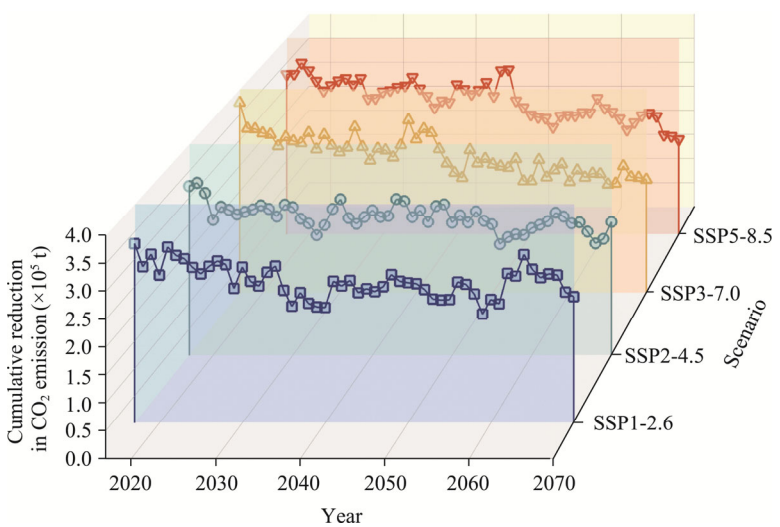

Fig. 10 Variations in CO_2 emission reductions from 2017 to 2070 under the SSP1-2.6, SSP2-4.5, SSP3-7.0, and SSP5-8.5 scenarios

4 Discussion

This study indicated that both temperature and precipitation in the Kaidu River Basin are expected to increase in the future, with temperature rising at a significantly faster rate than precipitation, particularly under the high emission scenario (SSP5-8.5). Furthermore, related research showed that the frequency of extreme high-temperature events in the basin will significantly increase, while extreme low-temperature events will decrease (Pan et al., 2022). Temperature and precipitation are critical factors influencing future runoff in the Kaidu River Basin. Under higher emission scenarios, the variability in temperature and precipitation is expected to increase, leading to a higher frequency of droughts and floods. Meanwhile, previous research suggested that the region may face more frequent extreme runoff events and more severe catastrophic floods in the future (Zheng et al., 2024). These changes present new challenges for the local hydropower sector. Firstly, the increased variability in runoff is likely to impact the efficiency and operational stability of hydropower plants, necessitating adjustments to current electricity generation scheduling strategies to cope with uncertain hydrological conditions. Secondly, the frequent occurrence of extreme climate events may escalate maintenance costs and increase the pressure of risk management on hydropower infrastructure, particularly in flood and drought prevention. To address these challenges, the local hydropower sector should adopt a range of adaptive measures. Investment should be made in more flexible and intelligent hydropower dispatch systems to enhance the ability to respond to runoff variability. Additionally, efforts should focus on strengthening climate data monitoring and analysis to improve the capacity to predict future climate trends, thereby optimizing resource planning and management. Finally, the hydropower sector should enhance collaboration with other relevant departments to develop comprehensive climate adaptation strategies, ensuring a transition to clean energy while maintaining the security and stability of power supply.

This study provides a scientific foundation for addressing climate change and optimizing water resource management, while also supporting clean energy transitions and sustainable regional economic development, which is critical for ensuring energy security and mitigating climate change risks. A recent research indicated that the Kaidu River Basin is likely to experience more frequent extreme climate events in the future (Zhang et al., 2024). Therefore, future research should focus on investigating the impact of climate variability on hydropower generation, particularly the potential effects of extreme climate events, such as droughts and heavy rainfall, on hydropower resources. These events could significantly affect reservoir level regulation, leading to seasonal variations in hydropower resources (Naz et al., 2018; Brás et al., 2023). Additionally, future studies should conduct sensitivity analyses of climate change on hydropower resources, quantitatively assessing the contributions of different climatic variables to hydropower output (Klein et al., 2013; Anghileri et al., 2018). This would provide policymakers with a more comprehensive understanding of how climate factors impact the hydropower system in the Kaidu River Basin. It is important to note that this study offers only preliminary estimates of electricity generation. Future research could incorporate reservoir operation models to more comprehensively simulate the electricity generation of two-reservoir, nine-step cascade hydropower stations in the Kaidu River Basin (Chong et al., 2021; Song et al., 2023), thereby offering deeper insights into future trends in hydropower resources within the basin.

5 Conclusions

Given the increasing frequency of extreme climate events, it is critical to analyze future changes in water resources and hydropower potential in the Kaidu River Basin. This study evaluated future runoff and hydropower availability under various climate change scenarios, with a focus on assessing their implications for CO_2 emission reductions. The key findings are as follows:

(1) Compared to the observational period, precipitation exhibits a slight increase under all four SSP scenarios. However, the three temperature variables (mean, maximum, and minimum

temperatures) demonstrate significantly more pronounced warming trends as greenhouse gas emission intensifies, with temperature increases far outpacing those in precipitation. This imbalance suggests a potential future characterized by water resource disparities and increased frequency of extreme climate events in the basin.

(2) Annual runoff exhibits a fluctuating declining trend under all emission scenarios, with sharper decreases observed under the higher emission scenario, particularly under the SSP5-8.5 scenario. Seasonally, runoff peaks in July and reaches its lowest point in March. These findings provide reliable data to inform water resource management in the Kaidu River Basin and contribute to forecasting water level fluctuations in the downstream of the Bosten Lake.

(3) Hydropower resources closely follow runoff trends, with the highest emission scenario (SSP5-8.5) exhibiting the most significant changes, highlighting the sensitivity of hydropower to climate change. Seasonally, summer remains the peak period for hydropower resources, while early spring represents the lowest point, with an observed advancement in the timing of the peak period. As hydropower potential declines, its capacity to reduce CO_2 emissions also diminishes. These findings emphasize the need for proactive measures to address climate change challenges and ensure the sustainable utilization of hydropower resources in the inland river basin of arid regions.

Conflict of interest

The authors declare that they have no known competing financial interests or personal relationships that could have appeared to influence the work reported in this paper.

Acknowledgements

This research was funded by the National Natural Science Foundation of China (42067062). We would like to sincerely thank Director ZHANG Yafeng and Director DU Jie from the Midstream Management Station of the Kaidu River for providing comprehensive hydropower station data as the foundation for this study and offering thoughtful guidance and tremendous support during the field investigation.

Author contributions

Conceptualization: XU Changchun, ZHANG Jing, WANG Hongyu; Data curation: ZHANG Jing, WANG Hongyu; Formal analysis: ZHANG Jing; Funding acquisition: XU Changchun; Investigation: ZHANG Jing, WANG Hongyu; Methodology: ZHANG Jing, LONG Junchen, WANG Yazhen; Project administration: XU Changchun; Resources: XU Changchun; Software: ZHANG Jing, WANG Hongyu, LONG Junchen; Supervision: XU Changchun, WANG Hongyu; Validation: ZHANG Jing, WANG Hongyu, WANG Yazhen; Visualization: ZHANG Jing, WANG Hongyu, LONG Junchen; Writing - original draft: ZHANG Jing; Writing - review & editing: XU Changchun. All authors approved the manuscript.

References

Anghileri D, Botter M, Castelletti A, et al. 2018. A comparative assessment of the impact of climate change and energy policies on alpine hydropower. Water Resources Research, 54(11): 9144–9161.

Asgari M, Yang W H, Lindsay J, et al. 2022. A review of parallel computing applications in calibrating watershed hydrologic models. Environmental Modelling & Software, 151(4): 105370, doi: 10.1016/j.envsoft.2022.105370.

Brás T A, Simoes S G, Amorim F, et al. 2023. How much extreme weather events have affected European power generation in

the past three decades? Renewable and Sustainable Energy Reviews, 183(2): 113494, doi: 10.1016/j.rser.2023.113494.

Castaneda-Gonzalez M, Poulin A, Romero-Lopez R, et al. 2023. Hydrological models weighting for hydrological projections: The impacts on future peak flows. Journal of Hydrology, 625(11): 130098, doi: 10.1016/j.jhydrol.2023.130098.

Chen Z S, Chen Y N, Li B F. 2013. Quantifying the effects of climate variability and human activities on runoff for Kaidu River Basin in arid region of Northwest China. Theoretical and Applied Climatology, 111: 537–545.

Chong K L, Lai S H, Ahmed A N, et al. 2021. Optimization of hydropower reservoir operation based on hedging policy using Jaya algorithm. Applied Soft Computing, 106: 107325, doi:10.1016/j.asoc.2021.107325.

Chuphal D S, Mishra V. 2023. Increased hydropower but with an elevated risk of reservoir operations in India under the warming climate. Science, 26(2): 105986, doi: 10.1016/j.isci.2023.105986.

Dallison R J H, Patil S D. 2023. Impact of climate change on hydropower potential in the UK and Ireland. Renewable Energy, 207: 611–628.

Donk P, Van Uytven E, Willems P, et al. 2018. Assessment of the potential implications of a 1.5°C versus higher global temperature rise for the Afobaka hydropower scheme in Suriname. Regional Environmental Change, 18: 2283–2295.

Fan M T, Xu J H, Chen Y N, et al. 2021. Modeling streamflow driven by climate change in data-scarce mountainous basins. Science of the Total Environment, 790(5): 148256, doi: 10.1016/j.scitotenv.2021.148256.

Fang G H, Li Z, Chen Y N, et al. 2023. Projecting the impact of climate change on runoff in the Tarim River simulated by the Soil and Water Assessment Tool Glacier model. Remote Sensing, 15(16): 3922, doi: 10.3390/rs15163922.

Hock R. 2003. Temperature index melt modelling in mountain areas. Journal of Hydrology, 282(1–4): 104–115.

Holanda P D S, Blanco C J C, Mesquita A L A, et al. 2017. Assessment of hydrokinetic energy resources downstream of hydropower plants. Renewable Energy, 101: 1203–1214.

IPCC (Intergovernmental Panel on Climate Change). 2015. Technology-specific Cost and Performance Parameters. In: Climate Change 2014: Mitigation of Climate Change: Working Group III Contribution to the IPCC Fifth Assessment Report. Cambridge: Cambridge University Press, 1329─1356.

IPCC. 2023. Climate Change 2023: Synthesis Report. Contribution of Working Groups I, II and III to the Sixth Assessment Report of the Intergovernmental Panel on Climate Change. Geneva: IPCC.

Jian H H. 2023. Assessment of hydroelectric potential under climate change and hydrological parameters based on soft-computing: A case study. Energy Reports, 9(3): 3035–3047.

Jing Z Q, Wang Y M, Chang J X, et al. 2024. Benefit compensation of hydropower-wind-photovoltaic complementary operation in the large clean energy base. Applied Energy, 354: 122040, doi: 10.1016/j.apenergy.2023.122040.

Kan B Y, Su F G, Xu B Q, et al. 2018. Generation of high mountain precipitation and temperature data for a quantitative assessment of flow regime in the Upper Yarkant Basin in the Karakoram. Journal of Geophysical Research: Atmospheres, 123(3): 8462–8486.

Klein D R, Olonscheck M, Walther C, et al. 2013. Susceptibility of the European electricity sector to climate change. Energy, 59: 183–193.

Li X D, Tan Z F, Shen J Y, et al. 2024. Research on the operation strategy of joint wind-photovoltaic-hydropower-pumped storage participation in electricity market based on Nash negotiation. Journal of Cleaner Production, 442(3): 140981, doi: 10.1016/ j.jclepro.2024.140981.

Liu F, Xu C C, Long Y X, et al. 2022. Assessment of CMIP6 model performance for air temperature in the arid region of Northwest China and subregions. Atmosphere, 13(3): 454, doi: 10.3390/atmos13030454.

Liu X C, Tang Q H, Voisin N, et al. 2016. Projected impacts of climate change on hydropower potential in China. Hydrology and Earth System Sciences, 20(8): 3343–3359.

Lohmann D, Raschke E, Nijssen B, et al. 1998. Regional scale hydrology: I. Formulation of the VIC–2L model coupled to a routing model. Hydrological Sciences Journal, 43(1): 131–141.

Luo M, Liu T, Meng F H, et al. 2019. Spatiotemporal characteristics of future changes in precipitation and temperature in Central Asia. International Journal of Climatology, 39(3): 1571–1588.

Melo L B, Estanislau F B G L e, Costa A L, et al. 2019. Impacts of the hydrological potential change on the energy matrix of the Brazilian State of Minas Gerais: A case study. Renewable and Sustainable Energy Reviews, 110(10163): 415–422.

Mohsin M, Orynbassarov D, Anser M K, et al. 2023. Does hydropower energy help to reduce CO_2 emissions in European Union countries? Evidence from quantile estimation. Environmental Development, 45(368): 100794, doi: 10.1016/j.envdev. 2022.100794.

Naz B S, Kao S C, Ashfaq M, et al. 2018. Effects of climate change on streamflow extremes and implications for reservoir inflow in the United States. Journal of Hydrology, 556(2): 359–370.

Pan Y M, Dai X R, Mao D L. 2022. Spatiotemporal variability of extreme climate events in the Kaidu River–Kongque River

Basin, Xinjiang, over the past 59 years. Hubei Agricultural Sciences, 61(15): 42–49, 74. (in Chinese)

Song Y, Shen C Q, Wang Y. 2023. Multi-objective optimal reservoir operation considering algal bloom control in reservoirs. Journal of Environmental Management, 344: 118436, doi: 10.1016/j.jenvman.2023.118436.

Su F, Zhang L, Ou T H, et al. 2016. Hydrological response to future climate changes for the major upstream river basins in the Tibetan Plateau. Global and Planetary Change, 136: 82–95.

Sun X S, Wang X G, Liu L P, et al. 2019. Development and present situation of hydropower in China. Water Policy, 21(3): 565–581.

Tuoheti S, Aji D. 2022. Impact of climate change in the Bosten Lake Basin on the Kaidu River runoff. Climate and Environmental Research, 27(2): 323–332. (in Chinese)

Ullah K, Raza M S, Mirza F M. 2019. Barriers to hydro-power resource utilization in Pakistan: A mixed approach. Energy Policy, 132: 723–735.

van Vliet M T H, Wiberg D, Leduc S, et al. 2016. Power-generation system vulnerability and adaptation to changes in climate and water resources. Nature Climate Change, 6: 375–380.

Wood E F, Lettenmaier D P, Zartarian V G. 1992. A land-surface hydrology parameterization with subgrid variability for general circulation models. Journal of Geophysical Research: Atmospheres, 97(D3): 2717–2728.

Wu J, Gao X J. 2013. A gridded daily observation dataset over China region and comparison with the other datasets. Chinese Journal of Geophysics, 56(4): 1102–1111. (in Chinese)

Xavier A C F, Martins L L, Rudke A P, et al. 2022. Evaluation of Quantile Delta Mapping as a bias-correction method in maximum rainfall dataset from downscaled models in São Paulo state (Brazil). International Journal of Climatology, 42(1): 175–190.

Yang L, Rojas J I, Montlaur A. 2020. Advanced methodology for wind resource assessment near hydroelectric dams in complex mountainous areas. Energy, 190: 116487, doi: 10.1016/j.energy.2019.116487.

Yuan X, Su C W, Umar M, et al. 2022. The race to zero emissions: Can renewable energy be the path to carbon neutrality? Journal of Environmental Management, 308(7645): 114648, doi: 10.1016/j.jenvman.2022.114648.

Zhang L L, Su F G, Yang D Q, et al. 2013. Discharge regime and simulation for the upstream of major rivers over Tibetan Plateau. Journal of Geophysical Research: Atmospheres, 118(15): 8500–8518.

Zhang W X, Clark R, Zhou T J, et al. 2024. 2023: Weather and climate extremes hitting the globe with emerging features. Advances in Atmospheric Sciences, 41(6): 1001–1016.

Zhang Y C, Li B L, Bao A M, et al. 2007. Study on snowmelt runoff simulation in the Kaidu River basin. Science in China Series D: Earth Sciences, 50: 26–35.

Zhao Y M, Dong N P, Li Z S, et al. 2021. Future precipitation, hydrology and hydropower generation in the Yalong River Basin: Projections and analysis. Journal of Hydrology, 602: 126738, doi: 10.1016/j.jhydrol.2021.126738.

Zheng P, Cheng Y N, Wang H J, et al. 2024. Impact of climate change on extreme runoff in the Tianshan region: A case study of the Kaidu River. Journal of Irrigation and Drainage, 43(4): 105–112. (in Chinese)

Zhong R D, Zhao T T G, He Y H, et al. 2019. Hydropower change of the water tower of Asia in 21st century: A case of the Lancang River hydropower base, upper Mekong. Energy, 179: 685–696.